Reconsidering astrophysical constraints on macroscopic dark matter

Jagjit Singh Sidhu and Glenn D. Starkman

Phys. Rev. D **101**, 083503 — Published 3 April 2020

DOI: 10.1103/PhysRevD.101.083503

Reconsidering astrophysical constraints on macroscopic dark matter

Jagjit Singh Sidhu, Glenn D. Starkman
Physics Department/CERCA/ISO Case Western Reserve University Cleveland, Ohio 44106-7079, USA

Macroscopic dark matter – "macros"– refers to a broad class of alternative candidates to particle dark matter with still unprobed regions of parameter space. These candidates would transfer energy primarily through elastic scattering with approximately their geometric cross-section. For sufficiently large cross-sections, the linear energy deposition could produce observable signals if a macro were to pass through compact objects such as white dwarfs or neutron stars in the form of thermonuclear runaway, leading to a type IA supernova or superburst respectively. We update the constraints from white dwarfs. These are weaker than previously inferred in important respects because of more careful treatment of the passage of a macro through the white dwarf and greater conservatism regarding the size of the region that must be heated to initiate runaway. On the other hand, we place more stringent constraints on macros at low cross-section, using new data from the Montreal White Dwarf Database. New constraints are inferred from the low mass X-ray binary 4U 1820-30, in which more than a decade passed between successive superbursts. Updated microlensing constraints are also reported.

I. INTRODUCTION

Dark matter is the most widely accepted explanation for cosmological and galactic dynamics (although see [1]), and yet very little is known about it beyond some upper limits on interaction cross-sections over a wide range of masses (see e.g [2]). New fundamental particles, not included in the Standard Model of particle physics, are popular candidates because they often arise in models of Beyond the Standard Model physics invented for independent reasons (e.g. the axion [3–5]). However, it remains an open possibility that dark matter is comprised instead entirely of macroscopic bound states of fundamental particles.

Such bound states could avoid strong constraints on the self-interactions of dark matter by virtue of their low number density instead of any intrinsic weakness of their non-gravitational couplings. One such open possibility is that dark matter is comprised of bound states of quarks or hadrons, as first proposed by Witten [6] as products of a first-order QCD phase transition, and later Lynn, Nelson, and Tetradis [7] and Lynn [8] again, who argued in the context of SU(3) chiral perturbation theory that a bound state of baryons with a well-defined surface may conceivably form in the presence of kaon condensation. This would place the dark matter squarely within the Standard Model. Others have suggested non-Standard Model versions of such nuclear objects and their formation, for example incorporating the axion [9].

Such states are referred to as "macros." A macro is then characterized by its geometric cross-section σ_χ and mass M_χ, which are related to the macro's average density ρ_χ

$$\sigma_\chi = 2.4 \times 10^{-10}\mathrm{cm}^2 \left(\frac{M_\chi}{g}\right)^{2/3} \left(\frac{\rho_{\mathrm{nuclear}}}{\rho_\chi}\right)^{2/3} . \quad (1)$$

Because of the exciting possibility that macros emerge from essentially the same Standard Model physics as ordinary nuclei, we regard $\rho_{\mathrm{nuclear}} = 3.6 \times 10^{14}\,\mathrm{g\ cm}^{-3}$ as a reference density of particular interest.

Due to their large mass and low number density, macro detectors must be extremely large or experience extremely long integration times to overcome the macros' extremely low flux compared to typical particle dark matter. Recent comprehensive assessments of limits on such macros as a function of their mass and cross-section [2, 10] identify large open windows in the parameter space.

For macro masses $M_x \leq 55\,\mathrm{g}$, careful examination of specimens of old mica for tracks made by passing dark matter [11, 12] has ruled out such objects as the primary dark-matter candidate (see Figure 1). For $M_x \geq 10^{24}\,\mathrm{g}$, a variety of microlensing searches have similarly constrained macros [13–16]. A large region of parameter space was constrained by considering thermonuclear runaways triggered by macros incident on white dwarfs [17]. Dark-matter-photon elastic interactions were used together with Planck cosmic microwave background (CMB) data to constrain macros of sufficiently high reduced cross-section σ_x/M_x [18]. Prior work had already constrained a similar range of parameter space, by showing that the consequence of dark-matter interactions with Standard Model particles is to dampen the primordial matter fluctuations and essentially erase all structures below a given scale (see e.g. [19]). The region of parameter space where macros would have produced a devastating injury similar to a gunshot wound on the carefully monitored population of the western world was also recently constrained [20].

Recently, together with collaborators, we suggested how ultra-high-energy cosmic-ray detectors that exploit atmospheric fluoresence could potentially be modified to probe parts of macro parameter space [21], including macros of nuclear density and intermediate mass. This analysis has led to constraints being placed using networks of cameras that were originally built to study bolides, i.e. extremely bright meteorites with absolute magnitude $M_v \leq -5$ [22]. We have also suggested how the approach applied to mica [11, 12] could be extended

to a larger, widely available sample of appropriate rock [23], and used to search for larger-mass macros.

There remains a wide range of parameters M_x and σ_x that are currently unconstrained by all the previously mentioned works. This includes a wide range of the nuclear-density line (1).

In this paper, we update certain astrophysical constraints on macro-dark-matter mass and cross-section. As in previous works, we consider dark matter of a single mass, even though a broad mass distribution is a reasonable possibility in the context of a composite dark-matter candidate.

The rest of this paper is organized as follows. In section II, we update constraints on macros from microlensing and femtolensing. In section III, we update constraints from the observation (or not) of Type Ia supernova events in white dwarfs (WDs), weakening previous contraints by more careful consideration of the propagation of the macro through the WD, and through greater conservatism regarding the minimum size region that must be heated above a critical temperature. On the other hand, we show that the large number of WD that have been collected from the literature in the Montreal White Dwarf Database [24] allow more stringent constraints to be placed on macros at low cross-sections. We also produce new constraints using arguments about thermonuclear runaway, by applying them to neutron stars (NSs), and the observation of superbursts. In the process, we rule out macros of "nuclear density" as the sole dark-matter candidate for certain mass ranges.

II. LENSING CONSTRAINTS

Massive objects passing between a light source and the Earth will gravitationally lens the source. For appropriately located objects of sufficient mass, the image can be measurably affected – it can be amplified, distorted, or even split into multiple images some of which are amplified and others de-amplified compared to the unlensed source. These effects are time-dependent, and can change over observationally accessible time-frames as the source-lens-observer geometry changes with the relative motion of elements.

A. Microlensing of M31

A recent seven-hour high-cadence observation of M31 (Andromeda), using the Subaru Hyper Suprime-Cam (HSC), was used to derive bounds for primordial black holes (PBHs) [25], based on the non-observation of a "lensing event" – the time-dependent amplification of a source star. The amount of dark matter that would be expected to pass through the "lensing tube" [26] during this observation can readily be calculated. For dark-matter candidates of a particular mass, the lensing tube represents the volume along the line-of-sight where the presence of a lens would cause a lensing event with amplification and duration greater than the appropriate threshold values for detectability.

Null lensing results allow constraints to be placed on the abundance of dark matter objects within a certain mass range, given the sensitivity of the measuring telescope. Objects that are too large or too small in mass would not be expected to produce observable lensing events. Objects of too-low mass produce lensing events with a low amplification. Morover, the duration of a lensing event is approximately the time it takes for the lens to cross its Einstein radius [25]

$$R_E = \sqrt{\frac{4GM_\chi}{\pi c^2} d \left(1 - \frac{d}{d_s}\right)}, \tag{2}$$

where d is the distance to the macro and $d_s \approx 770$kpc is the distance to M31. We assume for simplicity that the lens is in the Milky Way, so $d \ll d_s$. The crossing time

$$t_E \equiv \frac{R_E}{v} \approx 34min \left[\frac{M_{PBH}}{10^{-8}M_\odot} \frac{d}{100kpc} \frac{v}{200km/s}\right]^{\frac{1}{2}}. \tag{3}$$

Lensing events by low-mass objects are therefore brief, and likely to be missed between successive observations.

For a relatively short observational "campaign," objects that are too massive produce lensing events that are too long for the change in brightness of the lensed star to be detected. For the seven-hour long observation of M31 using Subaru Hyper Suprime-Cam (HSC), the maximum sensitivity to lensing events was for events with $t_{FWHM} \approx [0.07, 3]$ hours. With the mass density of dark matter fixed by galactic dynamics, the number of lensing events is also impacted by the number density of candidate dark matter lenses being inversely proportional to their mass.

Reference [25] has shown that diffraction effects become important and the maximum image magnification is significantly reduced for $M_{PBH} \lesssim 10^{23}\,$g, as the Schwarzchild radius of the PBH becomes smaller than the photon wavelength[1], with no constraints for $M_{PBH} \leq 10^{22}\,$g.

Since the microlensing interaction is purely gravitational, these results [25] are directly applicable to compact objects other than PBHs, such as macros. We may therefore rule out macros with $10^{22}\text{g} \leq M_\chi \leq 4 \times 10^{24}\text{g}$ as the dominant dark matter component. Above $M_\chi \leq 4\times10^{24}$, they have already been excluded by previous microlensing experiments (see [2] and references therein).

The microlensing constraint does not apply if the macro blocks a significant fraction of the light that would

[1] This does not mean that the Schwarzschild radius, R_s, can be interpreted as the effective radius of the lens – the typical impact parameter of photons involved in the lensing event is still R_E rather than R_s.

be amplified. This happens when the macro radius exceeds the Einstein radius. The microlensing bound therefore applies only to

$$\sigma_\chi \leq \frac{4GM_\chi}{c^2} d = 7 \times 10^{-4} \frac{M_\chi}{\mathrm{g}} \mathrm{cm}^2. \quad (4)$$

However, this value of σ_χ lies well within the region of parameter space already ruled-out by consideration of interactions between macros and CMB photons (shaded grey in Figure 1).

B. Femtolensing

Femtolensing refers to gravitational lensing where the angular separation between two lensed images of the same source is of order 10^{-15} arcseconds. The separate images cannot be resolved, however an interference pattern in the energy spectrum of background sources could be observable.

In [27], constraints were placed on the abundances of PBH with $10^{17}\,\mathrm{g} \lesssim M_{PBH} \lesssim 10^{20}\,\mathrm{g}$, from the non-observation of such interference patterns in gamma-ray bursts (GRBs). However, [28] revisited these constraints, taking into account the finite size of the GRB sources, among several additional corrections. As the emission size of the GRB grows, changes in the magnification spectrum are damped more strongly, until they eventually disappear once the emission size exceeds the Einstein radius. For realistic emission sizes of gamma ray sources – $a_s \geq 10^{10}$cm – the femtolensing constraint is removed entirely (see e.g. Figure 2 of [28]).

The discovery of a large number of sources with $a_s \leq 10^9$cm would allow limits to be placed [28] on the abundance of dark matter in compact objects with $10^{16} \leq M_{CO} \leq 10^{19}$g. The smaller the sources, the more stringent the constraints (see Figure 5 of [28]).

III. CONSTRAINTS FROM THERMONUCLEAR RUNAWAYS

Reference [29] showed that in a WD a sufficiently large localized injection of energy might trigger thermonuclear reactions. If a critical temperature were exceeded in a region of sufficient size, fusion of carbon atoms would initiate subsequent reactions before the heat was able to diffuse away. This chain reaction may lead to thermonuclear runaway, and the WD would undergo a type IA supernova explosion. The minimum temperature needed to trigger such reactions is [29] $T_{trig} \sim 3 \times 10^9$ K. The minimum size of the trigger region λ_{trig} depends on the local density. NSs can also exhibit thermonuclear runaway in the form of a superburst [30]. Thus, it may be that a similar mechanism could trigger a superburst in NSs.

Using the analysis of [29], the authors of [31] placed constraints on the abundance of PBHs in the mass range $10^{19} \lesssim M_{\mathrm{PBH}} \lesssim 10^{20}$g from the continued existence of old WDs. If a PBH traveled through a WD, the adjacent matter would be gravitationally accelerated toward its trajectory. Upon thermalization, the temperature would exceed T_{trig}. If the PBH was sufficiently massive, the size of this heated region would exceed λ_{trig}. Constraints were therefore placed on the abundance of PBHs of that or greater mass. However, it was subsequently shown [32] that the order-of-magnitude estimates employed by Graham *et al.* [31] likely constrained PBHs with masses that were too small to cause thermonuclear runaways. It is unlikely that thermonuclear runaway can constrain any significant portion of the PBH parameter space below $M_{PBH} \sim 10^{22}$ g.

Similar constraints were obtained [17] on dark matter that deposits energy in the WD by elastic scattering – objects that we term macros. Here the region of the WD that is heated above T_{trig} is potentially much larger, and so the limits are likely more robust. We will proceed with the formalism developed in [17, 31] to re-examine the regions of macro parameter space in which a macro would have produced observable consequences for WDs or NSs. We first constrain macros that would have initiated a superburst on a NS in a shorter time than that which occurs naturally. Next, we show the upper bound derived in [17] for macros triggering type IA supernovae in a WD is too stringent and derive a more accurate upper bound.

A. Size of the trigger region

In [29] λ_{trig} was calculated for 5×10^7g cm$^{-3} \leq \rho \leq 5 \times 10^9$g cm^{-3}; however, the outer regions of WDs have densities as low as 10^7g cm^{-3} and lower-mass WDs are nowhere denser than approximately 10^7g cm^{-3}. To extend the analysis to lower density, we will evaluate below the scaling relation between λ_{trig} and the local density – $\lambda_{trig} \propto \rho^{-2}$ – obtained in [31] by comparing the heat-diffusion rate to the carbon-fusion rate. Timmes and Woosley showed [29] that the resulting estimate of λ_{trig} was within a few per cent of the value obtained by simultaneously solving the hydrodynamics, nuclear kinetics and transport equations of the deflagration front as it propagates through the WD.

Nevertheless, it is still unclear how exactly type IA supernovae are initiated [33]. Thus, while the initiation of a deflagration flame may be a necessary condition for a type IA supernova, it may not be sufficient. We will proceed with the caveat that for the constraints produced in this section it must still be shown through simulations that those regions of macro parameter space can indeed produce catastrophic thermonuclear runaway. The situation is similar with NSs where the precise nature of the initiation of a superburst is unclear [30] and so in this case as well we also proceed with the understanding that the regions of macro parameter space constrained in this paper still need to be tested against simulations. We now re-derive the scaling relation from [31] and briefly

describe how we use it.

The characteristic time for heat to diffuse through (and out of) a region of size λ_{trig} is

$$\tau_{diffusion} \approx \frac{\lambda_{\rm trig}^2}{\alpha}\,, \tag{5}$$

where $\alpha = K/c_p\rho$ is the thermal diffusivity of the medium, c_p is the specific heat capacity, ρ is the density, $K \propto T^3/(\kappa\rho)$ is the thermal conductivity[34], and κ is the opacity of the dominant carrier of energy. For $\rho < 10^8$g cm^{-3}, photons are the dominant energy carriers. As most of the electrons are ionized, free-free transitions are the main source of opacity, and so [34] $\kappa \propto \rho$.

The mean free time between carbon-ion collisions (and consequently fusion reactions) is inversely proportional to the density,

$$\tau_{fusion} \sim (\sigma v n)^{-1}\,. \tag{6}$$

Since the size of the trigger region is obtained by requiring $\tau_{fusion} < \tau_{diffusion}$, $\lambda_{\rm trig} \propto \rho^{-2}$. For low density regions in a compact object, we use this scaling relation to calculate λ_{trig} using the results for the trigger size at the lowest density calculated in reference [29]. For high density regions, we use the numerical results for λ_{trig} already tabulated in reference [29].

The presence of iron-group impurities in the heavy-element ocean located near the surface of a NS reduces the number density of carbon ions. This increases the minimum column density that must be accreted for thermonuclear runaway to be achieved [35].

B. Energy deposition

As a macro passes through a compact object, it causes an initial rise in the temperature of the affected matter – from T_i to T_f – through elastic scattering. The magnitude of this temperature rise depends on the energy deposited per unit mass of white-dwarf or neutron-star material

$$\varepsilon_{in} = \int_{T_i}^{T_f} C_V dT\,, \tag{7}$$

where C_V is the specific heat. The usual temperature of a WD or NS is at most only $T_i \sim 1\,$keV. This is much less than T_{crit}, and so can be neglected.

The ions in a WD are non-degenerate and have specific heat [36]

$$C_{V,ions} = 3\frac{k_B}{\mu}\,, \tag{8}$$

where $\mu \approx 1.7 m_p$ is the mean molecular weight and m_p is the proton mass.

For large densities, $\rho \gtrsim 10^9 g cm^{-3}$, the Fermi energy approaches the thermal energy and C_V acquires a contribution from a relativistic degenerate electron gas [37]

$$C_{V,electrons} = \left(\frac{\pi^2 Z k_B}{A m_p}\right)\left(\frac{k_B T}{E_F}\right)\,. \tag{9}$$

Here Z is the average atomic number of the material, and A is the average nucleon number. The Fermi energy of the degenerate electron gas

$$E_F = 1.9 MeV \left(\frac{2Z}{A}\right)^{\frac{1}{3}} \rho_8^{\frac{1}{3}}\,, \tag{10}$$

with ρ_8 the density of that region of the compact object in units of 10^8g cm^{-3}. E_F is typically a few MeV for the range of densities where the degenerate-electron specific heat contributes significantly.

Using (8) and (9) in (7) we find,

$$3\frac{k_B T_f}{\mu} + \left(\frac{\pi^2 Z}{2A}\right)\frac{(k_B T_f)^2}{m_p E_F} = \varepsilon_{in}(v_x, \sigma_x, M_x)\,. \tag{11}$$

The first term on the left hand side dominates for $k_B T \lessapprox 1 MeV$, above which the second term dominates.

ε_{in}, and hence T_f, could depend on the velocity of the macro v_χ, e.g. in the case of elastic scattering. A macro that is incident on a WD or NS will have been gravitationally accelerated to much greater than its initial speed, thus

$$v_\chi \simeq v_{esc} \simeq \sqrt{\frac{2GM_{CO}}{r_{CO}}}\,, \tag{12}$$

where M_{CO} is the mass of the compact object and r_{CO} is the radius of the compact object. We have neglected relativistic corrections because, even for NSs, they are only 3%.

If the final temperature of the heated region $T \geq T_{crit} \sim 10^{10}\,$K, we expect some of this energy to be used in endothermic photodisintegration reactions. Thus, the size of the region with $T > T_{trig}$ is not expected to be much larger than σ_x. For example, at $T = 10^{10}\,$K, the carbon photodisintegration rate to three alpha particles (the reverse of the triple-alpha process) is $\sim 10^{10}\,$s^{-1}. The carbon fusion rate [38] at this temperature and $\rho = 10^7$ g cm^{-3} is $\sim$ few $\times 10^{10}\,$s^{-1}. However, due to the strong temperature dependence of these rates, fusion becomes the fastest process below $T \sim 10^{10}\,$K. We therefore expect the propagation of a deflagration flame to begin once the temperature drops below $T \sim 10^{10}\,$K

We require that the macro diameter be significantly larger than λ_{trig} (calculated as described in Section III A above)

$$\sigma_x > 10\frac{\pi}{4}\lambda_{trig}^2\,. \tag{13}$$

We adopt the factor of 10 to ensure that photodisintegration does not quench the deflagration flame – by requiring a region much larger than the trigger size to be heated above T_{trig}, we expect the propagation of a deflagration flame to be more likely. The requirement (13) is used to determine the lower bound on σ_x as can be seen in Figure 1, and discussed below in subsection C. 2.

We also demand that enough energy is deposited to raise that area σ_x above T_{trig}:

$$v_x > \sqrt{C_V T_{trig}} \gtrsim 6 \times 10^8 cms^{-1}\,. \tag{14}$$

As we will show in subsection C. 1, this is important in determining the maximum reduced cross-section σ_x/M_x that can be probed by considering thermonuclear runaways triggered at a particular depth within a compact object.

C. Elastic scattering bounds

We consider the bounds on the $\sigma_x - M_x$ parameter space from energy deposition by the macro into the compact-object through elastic scattering. We begin by showing that the maximum value of σ_x for the constrained region, previously obtained in [17] through the study of a population of WDs, was overly optimistic (i.e. too high); we derive a more accurate (lower) value. We also derive the analogous quantity for NSs, subject to some additional assumptions due to the more extreme nature of the environment compared to WDs.

Next, we determine the lower boundary of the constrained region (i.e. the smallest σ_x for each M_x), which is the minimum cross-section necessary to initiate the propagation of a deflagration flame in a WD or on the surface of a NS. Finally, we determine what mass ranges can be probed by each of WDs and NSs, to determine the constraints subject to the caveats described above.

Both WDs and NSs that are in binary systems can undergo thermonuclear runaway. WDs undergo a type IA supernova event if the WD accretes enough mass from its companion for its mass to reach the Chandrasekhar limit, the maximum possible white dwarf mass that can be supported by electron degeneracy pressure [39].

Unlike WDs, NSs will not explode catastrophically. The outer layer of a NS consists of an ocean of heavy elements including a significant amount of carbon at high densities ($\mathcal{O}$(100 m) below the surface). Ignition of this carbon layer can cause a NS to undergo a "superburst" [40]. These have been observed with recurrence times ranging from a few days to $\sim$ 10 years [30]. Typically, superbursts occur once the mass of the layer of carbon – formed from the accretion of hydrogen or helium onto the NS – reaches $\sim 10^{24}$g [35, 41]. Heat flowing out from the crust is deposited in the carbon "ocean" by electron capture and pycnonuclear reactions [41], augmenting compressional heating by the overlying material. Only once this much material has accumulated is the base of the carbon ocean hot enough to initiate a thermonuclear runaway. This yields a superburst energy of $\sim 10^{42}$ergs, assuming all the carbon ignites.

1. *Maximum constrained reduced cross-section*

The energy deposited through elastic scattering by a macro transiting a compact object is

$$\frac{dE}{dx} = \sigma_x \rho_{CO} v_x^2 \,, \tag{15}$$

where ρ_{CO} is the local density at a point within the compact object. v_x is a function of the depth of the macro in the compact object. The drag force experienced by a macro will decelerate it

$$a_x = \frac{GM_{CO}}{R_{CO}^2} - \frac{1}{2} C_d \rho_{CO} v_x^2 \sigma_x / M_x \,. \tag{16}$$

Here C_d is the drag coefficent, and depends on the Reynolds number, Re, of the flow

$$Re = \frac{\rho u L}{\mu_{dyn}} \,, \tag{17}$$

where $u = v_x$ is the relative velocity between the macro and the material of the compact object, $L = r_x$ is the characteristic length scale of the problem, and μ_{dyn} is the dynamical viscosity, which is not known for WDs or the outer regions of a NSs. For values suggested from theory [42], the range of Re for our purposes here is never low enough for the drag coefficient to deviate from the typical value for a sphere of $0.1 - 2$ [43]. However, for low values of Re, C_d could increase by several orders-of-magnitude, resulting in the macro experiencing a much higher drag force. If the dynamical viscosity is subsequently determined to be significantly higher, this would further reduce the parameter space that may be probed by thermonclear runaway. For now, we proceed with the most conservative value in the standard range, $\mathrm{C_d} = 2$, in producing our constraints.

To solve (16), which we do numerically, we must use a density profile for a typical compact object. We use the density profile of a typical WD [44] and of a typical NS crust [45] to simulate the evolution of the velocity of an incident macro for various values of σ_x/M_x. We then find the deepest point in the compact object where a macro of a certain reduced cross-section satisfies (14), having properly accounted for the column density encountered by the macro. The relevant point on the trajectory is the deepest point because that corresponds to the largest density along the trajectory of the macro where it satisfies equation (14) . This maximum density point then has the smallest value of λ_{trig}, because $\lambda_{trig} \propto \rho^{-2}$ (as discussed in Section III A). Consequently, per (13), this gives us the smallest cross-sections that can be constrained .

For macros with a sufficiently high σ_x/M_x, the macro is slowed down before it reaches the relevant depth in a compact object and is unable to transfer enough energy to trigger thermonuclear runaway. We find this limiting value of the reduced cross section to be $\sigma_x/M_x \gtrapprox 10^{-16}$ cm^{2}g^{-1} for WDs and $\sigma_x/M_x \gtrapprox 10^{-12}$ cm^{2}g^{-1} for NSs. However, there is a narrow range of values of σ_x/M_x around these two values where sufficient energy is transferred to initiate thermonuclear runaway that is dependent on where exactly in the compact object thermonuclear runaway is initiated.

The upper bound on the reduced cross-section for WDs is significantly smaller than that derived in [17]. In reference [17], the macro was assumed to be able to trigger a

type IA supernova once it penetrated the non-degenerate surface layer of a WD, which is typically narrow and much less dense than central densities. This assumption overestimated the parameter space that was constrained. For a given cross-section, σ_x, macros of too small a mass M_x were constrained. In this work, we have used a typical WD density profile from [44] to better estimate the true boundary from WDs. This is itself uncertain, since the radial density profile of WDs has not been determined definitively – the correct bound could lie above or below our bound, however, the upper bound in [17] is indeed an overestimate.

We find that NSs might "re-constrain" some of the parameter space that was previously ruled out by WDs. However, these NS constraints merit additional scrutiny due to the relativistic speeds reached by macros incident on the surface of a NS, $v \sim 0.7$c. We require that the macro not be destroyed in transiting the outer layers of the NS before reaching the heavy-element ocean. The exact constrained region therefore depends on the microphysics of the macro, and how tightly it is bound. We can get an estimate of the constraints by taking the macro to be made of baryons, and estimating that the logarithm of the binding energy per baryon E_b scales linearly with the logarithm of the density, between atomic density ($\rho_{atomic} \simeq 1 g/cm^{-3}$, $E_b \simeq 10$eV) and nuclear density ($\rho_{nuclear} \simeq 10^{14} g/cm^{-3}$, $E_b \simeq 1$MeV). This yields an expression for the scaling between binding energy and density

$$E_b \sim 10eV \left(\frac{\rho_x}{g/cm^{-3}}\right)^{\frac{3}{7}}, \tag{18}$$

where of course

$$\rho_x = \frac{3M_x\pi^{\frac{1}{2}}}{4\sigma_x^{\frac{3}{2}}}.$$

Crudely, we require the energy transferred to be less than the binding energy per baryon multiplied by the number of baryons in the macro

$$E_b \frac{M_x}{m_b} \geq \sigma_x v_x^2 \int \rho dL\,. \tag{19}$$

where $m_b < 940MeV$ is the mass of a baryon and $\int \rho dL$ is the integrated column density along the trajectory of the macro upto the point where the macro just satisfies (14). (This ignores the very definite possibility of ablation of the macro surface.) This enforces a bound similar to that found above, $\sigma_x/M_x \lesssim 10^{-11}$ cm^{2}g^{-1}. The exact constrained region depends on the microphysics of the macro and the details of how it is held together. However, the upper limit in σ_x on the constrained region comes from considering the drag on the macro through the overlying layers of the compact object, which is more stringent than the considerations of binding energy.

2. *Minimum cross-section of constraint region*

For the elastic-scattering mechanism, $\varepsilon_{in} = v_x^2 \sim v_C^2$, where $v_C \sim \sqrt{\frac{k_B T_f}{m_C}}$ is the speed of the carbon ions in the immediate vicinity of the macro and $v_x^2 \sim v_C^2$ because the speed of the impacted ions will be approximately that of the macros that impacted them. Thus, whether or not E_{trig} is reached depends – as discussed earlier – on the speed of the macro as it impacts the carbon atoms.

The lower bound on σ_x was determined using (13). Since $\lambda_{trig} \propto \rho^{-2}$, it varies along the trajectory of the macro through the WD or NS crust. For smaller values of σ_x/M_x the macro will decelerate to the minimum speed at which it can still trigger thermonuclear runaway at a greater depth, corresponding to a higher density, and consequently a smaller λ_{trig}. Given (13), for smaller values of σ_x/M_x, smaller values of σ_x can be probed. Requiring that the macro not lose appreciable kinetic energy through the non-degenerate surface layer of a WD is not a sufficient requirement for triggering thermonuclear runaway. For WDs, the trigger sizes are given in [29]. For NSs, λ_{trig} is now larger because the heavy element ocean in a NS is expected to be only $\sim 20\%$ carbon [35]. Thus, the mean free time between collisions of carbon atoms increases since the number density of carbon atoms decreases. The diffusion rate decreases because the number density decreases, although the specific heat and thermal conductivity aren't changed significantly. Thus, λ_{trig} increases.

For NSs, to obtain the most restrictive constraints, we take into consideration the evolution of the column density as matter is accreted from the companion in the binary system. As accretion proceeds, the underlying layers are compressed to higher densities. Thus, some time is required to form carbon of a certain minimum density. Although the maximum effective exposure time for the NS we use to place constraints is $T = 2.5$ yr (as discussed below), the denser the carbon, the shorter the period for which it is "exposed". Consequently, smaller cross-sections (corresponding to smaller λ_{trig} and higher densities) can only be probed for smaller-mass macros, which have higher fluxes.

For white-dwarf constraints, at the lower boundary of cross-sections, we will constrain significantly higher mass macros below than did [17]. This is simply a result of the increased total exposure obtained by using the sample of WDs in the MWDD [24].

3. *Mass bounds*

Mass constraints can be derived by considering the expected number of macros incident on a sample of WDs or NSs

$$N_{\rm events} = f\frac{\rho_{\rm DM}}{M_\chi} v_x \sum_{i=1}^{N_{\rm sample}} A_{{\rm gccs,i}} \Delta t_i\,. \tag{20}$$

Here f is the fraction of dark matter comprised of macros ρ_{DM} is the dark-matter density; M_x is the mass of the macro. For the i-th compact object in the sample: $A_{gccs,i} = \pi R_{CO,i}^2(1 + v_{esc,i}^2/v_x^2)$ is its gravitationally enhanced capture-cross-section (for a CO with radius $R_{CO,i}$ and surface escape velocity $v_{esc,i}$), while $v_x \sim 10^{-3}c$ is the macro velocity far from the surface; Δt_i is the object's exposure time.

For WDs, we use data from the MWDD [24] to place constraints on more massive macros. For each of a sequence of threshold central densities, corresponding to threshold masses, we apply (20) to all WDs in the MWDD with known lifetimes and masses exceeding the threshold. The constrained region in Figure 1 is the union of the constraints for all choice of minimum central density. The MWDD allows us to push the constrained region to higher masses than in [17] or certain cross-section ranges. Enlarging the MWDD to include more WDs with known lifetimes would extend the range of accessible masses at a given cross section.

For NSs, the monitoring of X-ray binaries can be used to constrain lower-mass macros. Since the low mass X-ray binary 4U 1820-30 exhibited back-to-back superbursts more than a decade apart [40], we will use it to place constraints on macros. This X-ray binary is located approximately 1 kpc from the Galactic center. The dark-matter density there is expected to be at least 20 times higher than in the solar neighborhood (see e.g. [46]), $\rho_{DM} \approx 10^{-17}\,\mathrm{g\ m^{-3}}$.

Since macro impacts are approximately a Poisson process, the probability $P(n)$ of n macro passages through a given NS over a given exposure time is

$$P(n; N_{events}) = \frac{(N_{events})^n}{n!} e^{-N_{events}}\,, \tag{21}$$

where N_{events} is the expected number of macro passages through that NS in that time,

$$N_{\rm events} = 2\times 10^{11} f \left(\frac{\rm g}{M_x}\right)\left(\frac{\delta t}{10{\rm yr}}\right)\left(\frac{A_{\rm gccs}}{2\times 10^8{\rm km}^2}\right). \tag{22}$$

As expected, $A_{gccs} = \pi(10km)^2(1+v_{esc}^2/v_x^2)$, with $v_{esc} \approx (2/3)c$. However, we must take care with determining the exposure time, δt. After a superburst from 4U 1820-30, it will take some time Δt to accrete sufficient column density y from its companion to support another superburst. $\Delta t = y\pi R_{NS}^2/\dot{M}$, with $\dot{M} \approx 10^{17} g s^{-1}$ the accretion rate onto 4U 1820-30. At a time T after the last superburst, the exposure time is $\delta t = \max(0, T - \Delta t)$. Although the time between superbursts was observed to be approximately one decade, the duty cycle of the instrument that observed these superbursts, RXTE-ASM, is around 40% [47]. Combined with spacecraft maneuvers that were planned to produce a highly stochastic pattern of sky coverage, a randomly chosen source was scanned typically 5 to 10 times per day [47], corresponding to an average time between scans of at most 5 hours. A typical superburst last around 3 hours [35]. This gives an effective duty cycle of $\sim 60\%$. Thus, there is a non-negligible chance that a superburst will be missed.

With this effective duty cycle of $\sim 60\%$, there is less than a 5% probability that we will miss all superbursts in a decade if there are at least 4 superbursts during this time. This yields

$$N_{\rm events} = 4\times 10^{10} f \left(\frac{\rm g}{M_x}\right)\left(\frac{\delta t}{2.5{\rm yr}}\right)\left(\frac{A_{\rm gccs}}{2\times 10^8{\rm km}^2}\right). \tag{23}$$

Since no events are observed in this time T, $N_{events} \geq 3$ may be ruled out at 95% confidence since $P(0; 3) = 0.05$; this corresponds to

$$M_x \leq 1\times 10^{10} f{\rm g}\,. \tag{24}$$

Another superburst constraint could potentially be derived by comparing the expected macro-induced rate for thermonuclear runaway in NSs to that observed. For a population of N_{NS} Milky Way NSs that are found in compact binaries and are accreting from a companion star, we expect

$$N_{events} = f N_{NS} \frac{\rho_{\rm DM}}{M_x} A_{\rm gccs} v_x t \tag{25}$$

macro-induced superbursts in time t. As before, if n superbursts have occured, where N_{events} were expected, and $P_{\rm Poisson}(n; N_{events}) \leq 0.05$, then that value of N_{events} is ruled out at the 95% level.

Currently, only 15 known NSs are known to have experienced a superburst [30]. As the data from observed superburst becomes better, we can expect to probe beyond $M_x = 5\times 10^{10}\,{\rm g}$. For example, the observation of 100 superbursters (Figure 12 of reference [48] indicates there are about 100 Low Mass X-ray Binaries and High Mass X-Ray Binaries respectively), each undergoing superbursts no more than twice annually, would allow $M_x \leq 10^{12}{\rm g}$ to be probed.

It should be noted, that it is possible that some of the superbursts that are observed are, in fact, macro-induced! However, absent an observable signature that distinguishes macro-induced superbursts from ordinary superbursts, the best we can do is put limits on macro-parameter space from the fact that superbursts aren't more common than observed.

We present our results in Figure 1. The blue region represents our revised constraints from WDs. The red region with no hatching represents constraints from observations [35] of 4U 1820-30. The red hatched region represents constraints that could eventually be inferred from monitoring of NSs in X-ray binaries. The lower bounds are in general determined by (13), where λ_{trig} is bigger for NSs than WDs as discussed in Section III C. 2. The mass bounds are determined as in Section III C. 3, by requiring that at least one macro transit should have occurred and triggered thermonuclear runaway. Finally, the slanted upper bounds are determined by requiring that the criterion (14) be satisfied. This criterion can be

satisfied by macros with different $\sigma_{x,min}$ for different values of σ_x/M_x. This is because these macros can satisfy (14) at shallower depths in a compact object.

IV. CONCLUSION

We have applied the analyses of [17] and [25] to macros and identified the regions of cross-section-versus-mass parameter space that can be excluded based on: microlensing of stars in M31, superbursts in NSs, and type IA supernova in old WDs. Of particular interest, parts of the nuclear-density line in that parameter space have been ruled out. However, there remain three windows for nuclear density macros: $55\,\mathrm{g} \lesssim M_X \lesssim 10^3\,\mathrm{g}$, $5\times10^4\,\mathrm{g} \lesssim M_X \lesssim 10^8\,\mathrm{g}$, and $10^{10}\,\mathrm{g} \lesssim M_X \lesssim 10^{18}\,\mathrm{g}$ A substantial portion of the parameter space above and below nuclear density remains unconstrained. The atomic-density line is ruled out, except for a small window between 10^{20}g and 10^{22}g.

We reiterate that certain constraints reported here are subject to additional scrutiny because it is not certain that the conditions identified in [29] are indeed sufficient to initiate thermonuclear runaway, i.e. there remains some uncertainty whether in fact heating a region of size at least λ_{trig} to $T \sim$ few $\times10^9$ K necessarily causes type 1A supernovae in WDs and superbursts in NSs. We have exercised additional conservatism compared to past analyses in deploying that condition (by taking a larger λ_{trig}), however, future simulations of the relevant systems could refine or eliminate the associated constraints.

ACKNOWLEDGMENTS

This work was partially supported by Department of Energy grant de-sc0009946 to the particle astrophysics theory group at CWRU. JSS thanks Saurabh Kumar and David Cyncynates for helpful discussions.

[1] F. Lelli, S. S. McGaugh, and J. M. Schombert, The Astronomical Journal **152**, 157 (2016).
[2] D. M. Jacobs, G. D. Starkman, and B. W. Lynn, Monthly Notices of the Royal Astronomical Society **450**, 3418 (2015).
[3] R. D. Peccei and H. R. Quinn, Phys. Rev. Lett. **38**, 1440 (1977).
[4] S. Weinberg, Phys. Rev. Lett. **40**, 223 (1978).
[5] F. Wilczek, Phys. Rev. Lett. **40**, 279 (1978).
[6] E. Witten, Physical Review D **30**, 272 (1984).
[7] B. W. Lynn, A. E. Nelson, and N. Tetradis, Nuclear Physics B **345**, 186 (1990).
[8] B. W. Lynn, "Liquid phases in SU(3) Chiral Perturbation Theory: Drops of Strange Chiral Nucleon Liquid and Ordinary Chiral Heavy Nuclear Liquid," (2010), arXiv:1005.2124.
[9] A. R. Zhitnitsky, JCAP **0310**, 010 (2003).
[10] D. M. Jacobs, A. Weltman, and G. D. Starkman, Physical Review D **91**, 115023 (2015).
[11] A. De Rujula and S. L. Glashow, Nature **312**, 734 (1984).
[12] P. B. Price, Physical Review D **38**, 3813 (1988).
[13] C. Alcock *et al.*, The Astrophysical Journal **550**, L169 (2001).
[14] P. Tisserand *et al.*, Astronomy & Astrophysics **469**, 387 (2007).
[15] B. J. Carr, K. Kohri, Y. Sendouda, and J. Yokoyama, Physical Review D **81**, 104019 (2010).
[16] K. Griest, A. M. Cieplak, and M. J. Lehner, Physical Review Letters **111**, 181302 (2013).
[17] P. W. Graham, R. Janish, V. Narayan, S. Rajendran, and P. Riggins, Phys. Rev. D **98**, 115027 (2018).
[18] R. J. Wilkinson, J. Lesgourgues, and C. Boehm, JCAP **4**, 026 (2013).
[19] C. Bœhm, P. Fayet, and R. Schaeffer, Physics Letters B **518**, 8 (2001).
[20] J. S. Sidhu, R. J. Scherrer, and G. Starkman, "Death by dark matter," (2019), arXiv:1907.06674.
[21] J. S. Sidhu, R. M. Abraham, C. Covault, and G. Starkman, JCAP **1902**, 037 (2019).
[22] J. S. Sidhu and G. Starkman, "Macroscopic dark matter constraints from bolide camera networks," (2019), arXiv:1908.00557.
[23] J. S. Sidhu, G. Starkman, and R. Harvey, Physical Review D **100** (2019).
[24] P. Dufour, S. Blouin, S. Coutu, M. Fortin-Archambault, C. Thibeault, P. Bergeron, and G. Fontaine, in *20th European White Dwarf Workshop*, Astronomical Society of the Pacific Conference Series, Vol. 509, edited by P.-E. Tremblay, B. Gaensicke, and T. Marsh (2017) p. 3, arXiv:1610.00986 [astro-ph.SR].
[25] H. Niikura *et al.*, Nature Astronomy **3**, 524 (2019).
[26] K. Griest, The Astrophysical Journal **366**, 412 (1991).
[27] A. Barnacka, J.-F. Glicenstein, and R. Moderski, Physical Review D **86**, 043001 (2012).
[28] A. Katz, J. Kopp, S. Sibiryakov, and W. Xue, Journal of Cosmology and Astroparticle Physics **2018**, 005 (2018).
[29] F. X. Timmes and S. E. Woosley, The Astrophysical Journal **396**, 649 (1992).
[30] J. in 't Zand, "Understanding superbursts," (2017), arXiv:1702.04899.
[31] P. W. Graham, S. Rajendran, and J. Varela, Physical Review D **92**, 063007 (2015).
[32] P. Montero-Camacho, X. Fang, G. Vasquez, M. Silva, and C. M. Hirata, Journal of Cosmology and Astroparticle Physics **2019**, 031 (2019).
[33] F. K. Röpke, in *Handbook of Supernovae* (Springer International Publishing, 2017) pp. 1185–1209.
[34] R. Kippenhahn and A. Weigert, *Stellar Structure and Evolution (Astronomy and Astrophysics Library)* (Springer, 1994).
[35] T. E. Strohmayer and E. F. Brown, The Astrophysical Journal **566**, 1045 (2002).
[36] S. Balberg and S. L. Shapiro, arXiv preprint astro-ph/0004317 (2000).

[37] A. Cumming and L. Bildsten, The Astrophysical Journal **559**, L127 (2001).
[38] G. R. Caughlan and W. A. Fowler, Atomic Data and Nuclear Data Tables **40**, 283 (1988).
[39] S. W. Hawking and W. Israel, *Three Hundred Years of Gravitation* (Cambridge University Press, 1989).
[40] J. in't Zand, M. Serino, N. Kawai, and C. Heinke, The Astronomer's Telegram **3625** (2011).
[41] A. Cumming and L. Bildsten, The Astrophysical Journal **559**, L127 (2001).
[42] S. Dall'Osso and E. M. Rossi, Monthly Notices of the Royal Astronomical Society **443**, 1057 (2014).
[43] Z. Duan, B. He, and Y. Duan, Scientific Reports **5** (2015), 10.1038/srep12304.
[44] F. X. Timmes, http://cococubed.asu.edu/code_pages/coldwd.shtml, accessed: 2018-09-30.
[45] B. Datta, A. V. Thampan, and D. Bhattacharya, Journal of Astrophysics and Astronomy **16**, 375 (1995).
[46] M. Cirelli *et al.*, Journal of Cosmology and Astroparticle Physics **2011**, 051 (2011).
[47] A. M. Levine, H. Bradt, W. Cui, J. G. Jernigan, E. H. Morgan, R. Remillard, R. E. Shirey, and D. A. Smith, The Astrophysical Journal **469**, L33 (1996).
[48] H.-J. Grimm, M. Gilfanov, and R. Sunyaev, Astronomy & Astrophysics **391**, 923 (2002).
[49] D. Cyncynates, J. Chiel, J. Sidhu, and G. D. Starkman, Physical Review D **95**, 063006 (2017).

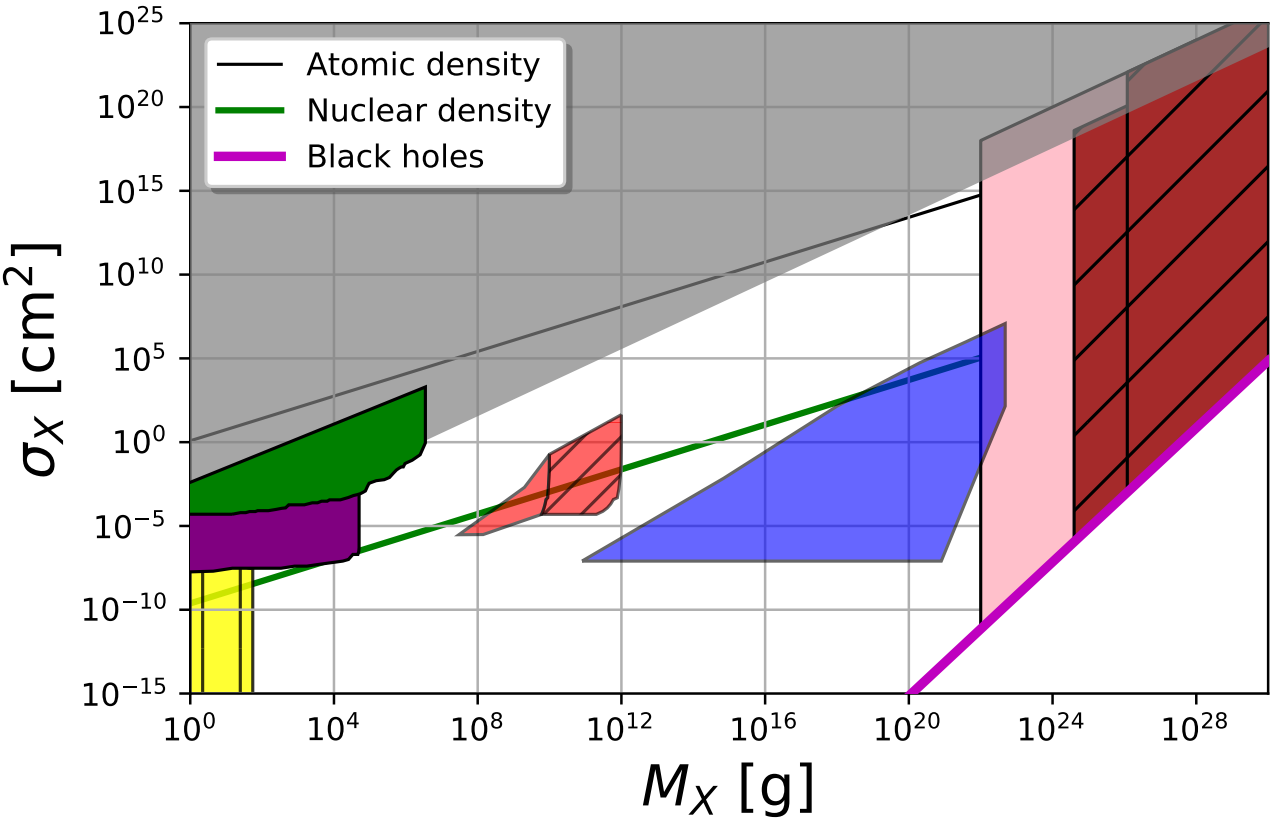

Figure 1. Figure 3 of [49] with the updated constraints discussed in the text. Objects within the region in the bottom-right corner should not exist as they would simply be denser than black holes of the same mass. The grey region is ruled out from structure formation [18]; the yellow from mica observation [11, 12]; the red from superbursts in NSs (this work – the hatched region representing potential future constraints); the dark blue from WDs becoming supernovae ([17] as revised in this work); the purple from a lack of human injuries or deaths [20]; the green from a lack of fast-moving bolides [22]; the maroon from a lack of microlensing events toward the Large Magellanic Cloud and the Galactic center [13–16], and, in pink, toward M31 [25].